ORIGINAL ARTICLE

Spray-dried sol-gel glass-ceramic powders based on the tunable thermal expansion of quartz and keatite solid solutions

Alessio Zandona[1] | Gundula Helsch[1] | Aurina Martínez Arias[2] | Alfred P. Weber[2] | Joachim Deubener[1]

[1]Institute of Non-Metallic Materials, Clausthal University of Technology, Clausthal-Zellerfeld, Germany

[2]Institute of Particle Technology, Clausthal University of Technology, Clausthal-Zellerfeld, Germany

Correspondence
Alessio Zandona, Institute of Non-Metallic Materials, Clausthal University of Technology, Clausthal-Zellerfeld, Germany.
Email: alessio.zandona@tu-clausthal.de

Abstract

Lithium aluminosilicate glass-ceramic powders were synthesized by the heat treatment of spray-dried sol-gel glassy nanobeads, obtaining quartz solid solution (Qss) and keatite solid solution (Kss) crystals. Their composition ranged between 75 mol% SiO_2 and pure silica along the spodumene join. The metastable crystals displayed tunable coefficients of thermal expansion ranging from $+30 \times 10^{-6}$ to -2.7×10^{-6} K^{-1} at room temperature, as obtained from their crystallographic characterization. The solid solution boundaries of Kss could be extended to 85 mol% SiO_2. Concurrently, X-ray diffraction measurements performed in situ at high temperature and at cryogenic conditions confirmed the known linear shift of the high-low quartz inversion temperature upon increasing Al+Li doping. The obtained results qualify aerosol synthesis as a very versatile method for the production of glass-ceramic powders in the LAS system.

KEYWORDS
glass-ceramics, quartz solid solution, sol-gel, spray-drying, thermal expansion

1 | INTRODUCTION

The availability of materials that can comply with stringent thermal expansion specifications is essential for numerous technological applications, spanning from electronic packaging to dental restoration.[1,2] In many of these cases, a macroscopic adjustment of the coefficient of thermal expansion (CTE) can be attained through the formulation of composite materials, relying on the combination of the properties of multiple phases. Solids exhibiting low or negative thermal expansion therefore represent a cornerstone of this approach[3,4]; within

this specific class of materials, lithium aluminosilicate (LAS) crystals arguably count among the oldest and best investigated.[5]

The structure of high quartz and keatite, two SiO_2 polymorphs with CTEs respectively close to zero and negative,[6,7] is indeed stabilized by a coupled Al+Li stuffing over increasingly wide temperature ranges down to the endmembers β-eucryptite ($LiAlSiO_4$) and β-spodumene ($LiAlSi_2O_6$).[8,9] Notably, the structural and thermal expansion characteristics of these phases ($Li_xAl_xSi_{1-x}O_2$) display a continuous variation as a function of composition.[10,11] Quartz solid solutions (Qss) and keatite solid

solutions (Kss) have been therefore appreciated for decades as the main crystalline constituents of zero thermal expansion glass-ceramics, in which they typically precipitate from a multicomponent parent glass.[12] Negative thermal expansion is instead generally not attainable in the compositionally analogous magnesium aluminosilicate (MAS) system, since the available silicate phases, that is, Mg-bearing Qss at low temperatures and indialite/cordierite at high temperatures, exhibit CTEs going from slightly to noticeably positive values in the absence of additional dopants.[13,14]

Several attempts to synthesize LAS powders or monoliths via the sol-gel route are also reported in the literature, particularly stressing the technical difficulties related to the drying and densification stages[15–19]; the possibility of applying Qss thin films on glass surfaces by dip-coating has also been examined.[20] Spray-drying is an established method for a controlled and easily upscalable synthesis of ceramic catalysts, food and pharmaceutical products.[21–24] Although its potential use in the formulation of glasses and glass-ceramics has been only limitedly explored so far,[25–29] we have recently described the production of functional glass-ceramic nanobeads based on the photocatalytic properties of $TiO_2(B)$ and anatase crystals.[30] In the present work, we further demonstrate the versatility of the spray-drying method by synthesizing a series of LAS glass-ceramic powders exhibiting compositionally tunable CTEs at room temperature, from mildly negative to strongly positive. Our detailed crystallographic characterization particularly reveals how this novel synthesis route enables to access virtually any Qss stoichiometry in the studied system and, in the case of Kss, to even enlarge the known compositional boundaries of the available solid solutions.

2 | EXPERIMENTAL SECTION

2.1 | Preparation of the glassy nanobeads

The target compositions of the 10 samples synthesized within this work are reported in Table 1. Tetraethoxysilane (TEOS, ≥99%, Fluka) was pre-hydrolyzed in isopropanol with a stoichiometric amount of deionized water, using HNO_3 (1 M, ≥99%, Fluka) to set the pH to ≈1. A Li_2O excess (2.5% of the molar SiO_2 content) was introduced by adding $LiNO_3$ (≥98%, Merck), with the intent of facilitating the formation of Qss in the resulting glasses, as from previous observations.[31] Suitable amounts of $LiNO_3$ and $Al(NO_3)_3 \cdot 9H_2O$ (≥98.5%, Merck) were then solved 1:1 in deionized water and added to the first solution under constant stirring, further diluting it with deionized water to 5 wt% equivalent total oxide content. As similarly detailed elsewhere,[30] 50 ml of the so-obtained mixture were then spray-dried in 2 h to obtain ~2 g of amorphous nanobeads. The solution was thereby nebulized by an aerosol atomizer (Atomizer, AGK 2000, Palas) operated with pressurized air (2.9 bar) into a tube furnace set at 500°C. A particle filter placed at the other extremity of the furnace allowed to retrieve the powders, which were then subjected to a further heat treatment at 500°C for 1.5 h to complete the decomposition of the precursors.

2.2 | Heat treatments

All samples were crystallized at 760°C for 30 min in a lab furnace to obtain glass-ceramics containing prevalently Qss; this temperature was selected after some explorative high-temperature X-ray diffraction (HT-XRD) measurements, aiming at maximizing the crystallinity of

TABLE 1 Nominal compositions (mol%) of the spray-dried glasses, which contained a Li_2O excess to foster the formation of quartz solid solutions (Qss).[31] The actual target stoichiometry of the Qss and keatite solid solution (Kss) phases forming in the samples, controlled by the Al/Si ratio of the glass, is additionally reported

| | Glass composition | | | |
Sample	Li_2O (mol%)	Al_2O_3 (mol%)	SiO_2 (mol%)	Target Qss/Kss stoichiometry
LA00	2.4	0.0	97.6	100 SiO_2
LA05	4.8	2.4	92.8	2.5 $Li_2O \cdot$ 2.5 $Al_2O_3 \cdot$ 95 SiO_2
LA10	7.1	4.9	88.0	5.0 $Li_2O \cdot$ 5.0 $Al_2O_3 \cdot$ 90 SiO_2
LA15	9.4	7.4	83.2	7.5 $Li_2O \cdot$ 7.5 $Al_2O_3 \cdot$ 85 SiO_2
LA18	10.8	8.8	80.4	9.0 $Li_2O \cdot$ 9.0 $Al_2O_3 \cdot$ 82 SiO_2
LA19	11.3	9.3	79.4	9.5 $Li_2O \cdot$ 9.5 $Al_2O_3 \cdot$ 81 SiO_2
LA20	11.8	9.8	78.4	10.0 $Li_2O \cdot$ 10.0 $Al_2O_3 \cdot$ 80 SiO_2
LA21	12.2	10.3	77.5	10.5 $Li_2O \cdot$ 10.5 $Al_2O_3 \cdot$ 79 SiO_2
LA22	12.7	10.8	76.5	11.0 $Li_2O \cdot$ 11.0 $Al_2O_3 \cdot$ 78 SiO_2
LA25	14.1	12.3	73.6	12.5 $Li_2O \cdot$ 12.5 $Al_2O_3 \cdot$ 75 SiO_2

the powders (see Figure 2A for an example). In the case of samples LA15 and LA10, another heat treatment was additionally applied to maximize the amount of Kss obtainable in the materials. The two samples, already crystallized at 760°C, were heated with a rate of 10 K min^{-1} respectively to 850 and 1050°C in the HTK 1200N heating chamber (Anton Paar) mounted on our diffractometer (see following). HT-XRD measurements were run in parallel to monitor the Qss–Kss transformation, which was concluded after ≈30 min in both cases.

2.3 | Transmission electron microscope (TEM)

Samples LA05 and LA20, both in the untreated and crystallized form, were dispersed in ethanol and deposited on carbon-coated copper grids. They were measured in a JEOL JEM2100 TEM, operated at 160 kV.

2.4 | X-ray diffraction (XRD)

Crystallographic characterization of the samples was performed using a Panalytical Empyrean diffractometer, mounting a Cu X-ray tube operated at 40 kV and 40 mA and a PIXcel 1D detector (255 channels, 14 mm active length). Silicon (≈5 wt%) was added as internal standard to each powder to facilitate the determination of lattice parameters, performed by Rietveld refinements using the software HighScore Plus (Malvern Panalytical). Relative

length changes in the crystals were averaged over all directions in the unit cell according to Equation (1):

$$\frac{\Delta l(T)}{l} = \frac{\left[((a(T))^2 \cdot c(T) \right]^{\frac{1}{3}} - \left[a_{ref}^2 \cdot c_{ref} \right]^{\frac{1}{3}}}{\left[a_{ref}^2 \cdot c_{ref} \right]^{\frac{1}{3}}}, \quad (1)$$

where $a(T)$ and $c(T)$ stand for the length of the respective lattice parameter obtained at temperature T and a_{ref} and c_{ref} for the reference values at room temperature.

The powders were found to be virtually fully crystalline using a weighed-in CaF_2 standard, that is, the residual amorphous fraction was estimated as <5 wt%. Rietveld refinements also enabled to estimate the relative mass fractions (wt%) of the main crystalline phases and the average crystallite size of the Qss crystals, determined with respect to a LaB_6 standard (NIST 660a). Room temperature measurements were performed on an adjustable x-y-z platform with a back-loading powder holder (10–90° 2θ, 0.026° 2θ stepsize, 50 s per step). Between 50 and 650°C, the data (15–80° 2θ, 0.026° 2θ stepsize, 50 s per step) were collected by heating the powders in Al_2O_3 crucibles using a HTK 1200N heating chamber (Anton Paar), whose calibration was described elsewhere.[20] Below ambient, the measurements (15–80° 2θ, 0.026° 2θ stepsize, 50 s per step) were performed in a TTK 600 chamber (Anton Paar) cooled with liquid N_2 and operated in vacuum or in N_2 atmosphere, as tested in a previous publication.[32] For this latter investigation, the powders were mixed with some Apiezon N cryogenic vacuum grease (Demaco), creating a paste that was then applied on the metallic sample holder.
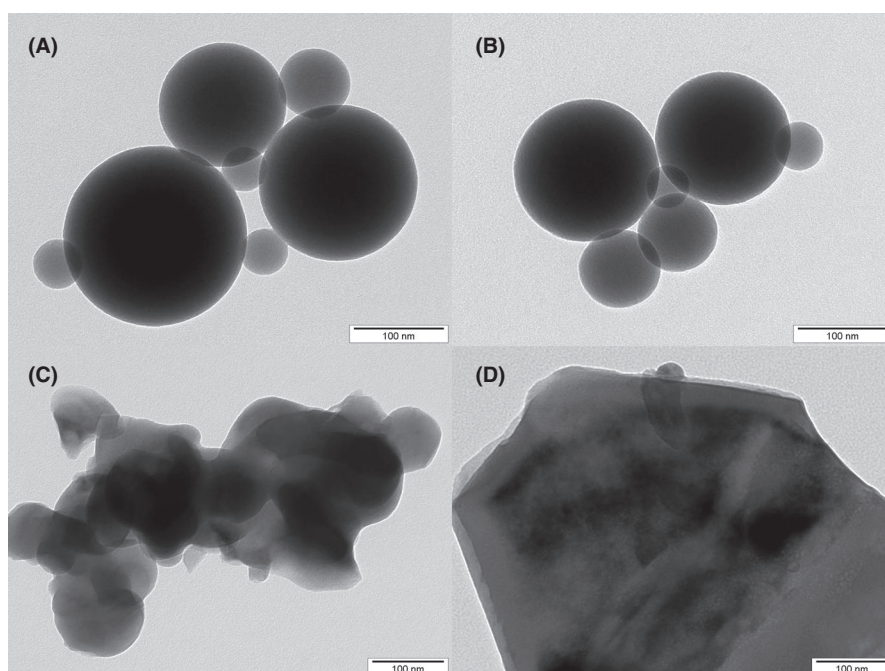

FIGURE 1 TEM micrographs of: (A) sample LA05 and (B) sample LA20, after the preliminary calcination at 500°C; (C) sample LA05 and (D) sample LA20, after crystallization heat treatments at 760°C

3 | RESULTS

3.1 | Microscopic characterization

The morphology of the spray-dried materials was characterized by transmission electron microscopy (TEM) (Figure 1). After a calcination at 500°C, the amorphous powders still consisted of nanobeads with a radius ranging from 20 to 100 nm, as similarly reported for SiO_2-TiO_2 glass-ceramics.[30] On the contrary, the crystallization heat treatment at 760°C induced extensive agglomeration and sintering, leading to the formation of irregularly shaped grains and slabs, in agreement with early studies on spray-dried aluminosilicate powders.[28]

3.2 | Quartz solid solutions

X-ray diffraction (XRD) measurements of the materials treated at 760°C revealed that the powders were virtually fully crystalline, as suggested by preliminary explorative HT-XRD measurements (Figure 2A); metastable Qss was invariably the predominant phase. However, Li_2O- and Al_2O_3-richer samples developed a non-negligible fraction of Kss (Table 2 and Section 3.3). All diffraction peaks shifted to lower 2θ angles with increasing Al_2O_3 and Li_2O doping (Figure 2B), due to the related expansion of the unit cells of both Qss and Kss. Weak reflections assignable to Li-metasilicate (Li_2SiO_3) and Li-disilicate ($Li_2Si_2O_5$) were additionally detected in all samples, most likely

originating from the slight Li_2O excess added to the glass stoichiometry to foster the formation of Qss.[31] Due to their low total amount (invariably <5 wt%) and broad diffraction features, these secondary phases were excluded from the Rietveld refinements, to avoid a possibly adverse impact on the reliability of the Qss and Kss lattice parameters determination.

Average crystallite sizes computed from Rietveld refinements did not display a definite trend and invariably resulted between 50 and 80 nm, possibly mirroring the average size of the initial glassy nanobeads. The room-temperature lattice parameters of Qss, instead, agreed closely with the values obtained from literature (Figure 3), confirming that the stoichiometry of the crystals (Table 1) could be essentially controlled by adjusting the Al/Si ratio of the parent glass, as shown previously.[31,32] The known transition from a low-quartz-like (LQss) to a high-quartz-like (HQss) structure was particularly evident in the trend displayed by the c lattice parameter, whose value increased steadily in the range 100–82.5 mol% SiO_2 and subsequently displayed a persistent stagnation at lower SiO_2 contents.[7,32,33]

We monitored the LQss-HQss transformation also as a function of temperature, as detailed in Figure 4: the positive expansion of trigonal LQss brought about a visible gradual peak shift to the left, which ceased as soon as the crystals assumed the high-temperature hexagonal symmetry of HQss, whose thermal expansion typically approaches zero. The phase transition was also emphasized by evident intensity changes; the determined critical

TABLE 2 Relative crystalline fractions, lattice parameters, and average crystallite sizes of quartz solid solution (Qss) and keatite solid solution (Kss) obtained from Rietveld refinements (neglecting minor secondary phases) of X-ray diffraction measurements performed at room temperature. The critical inversion temperatures (T_c) of Qss are also reported, as inferred from the expansion curves in Figure 5. In the column "Other phases": m for Li_2SiO_3, d for $Li_2Si_2O_5$, c for cristobalite

| Sample | Qss | | | | | Kss | | | | Other phases |
	wt%	a (Å)	c (Å)	Cr. size (nm)	T_c (°C)	wt%	a (Å)	c (Å)	Cr. size (nm)	
LA00	100	4.9195 (7)	5.408 (1)	51 (5)	565 (10)					m,d
LA05	100	4.9745 (6)	5.4190 (9)	64 (6)	365 (10)					m,d
LA10	100	5.0239 (7)	5.432 (1)	78 (8)	255 (10)					m,k
LA15	76 (4)	5.0919 (9)	5.448 (1)	74 (7)	90 (10)	24 (2)				m
LA18	76 (4)	5.1286 (5)	5.4571 (9)	72 (7)	−15 (10)	24 (2)				m
LA19	86 (4)	5.1364 (7)	5.457 (1)	69 (7)	−45 (10)	14 (1)				m
LA20	71 (4)	5.1449 (5)	5.4574 (9)	75 (7)	−70 (10)	29 (3)	7.505 (2)	9.040 (3)	62 (6)	m
LA21	60 (3)	5.1504 (6)	5.458 (1)	74 (7)	−100 (10)	40 (4)	7.507 (2)	9.051 (3)	59 (6)	m
LA22	78 (4)	5.1579 (6)	5.457 (1)	63 (6)	−135 (10)	22 (2)				m
LA25	66 (3)	5.1697 (6)	5.457 (1)	66 (7)	<−165	34 (3)	7.517 (2)	9.082 (4)	53 (5)	m
LA10, 1050°C	24 (2)					44 (4)	7.483 (2)	8.988 (3)	54 (5)	c,m
LA15, 850°C	6 (1)					88 (4)	7.482 (1)	9.011 (2)	68 (7)	d
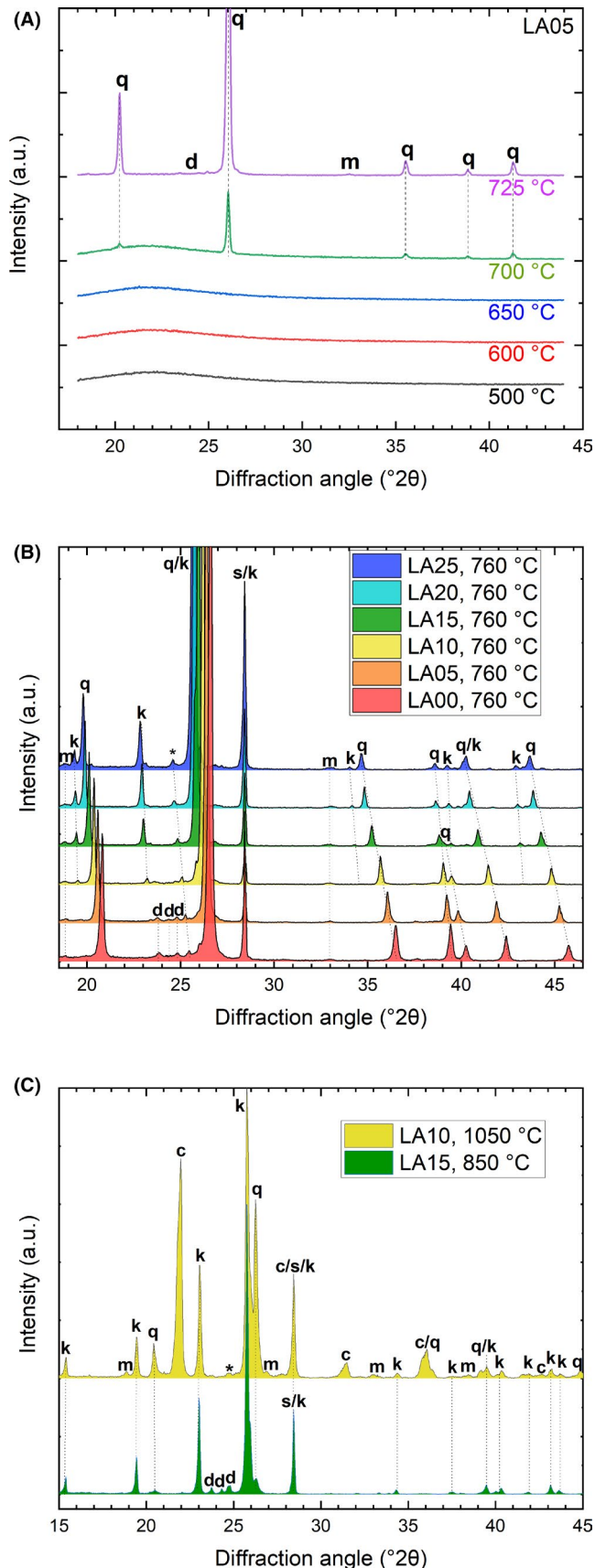
FIGURE 2 (A) Crystallization of sample LA05 monitored by in situ high-temperature X-ray diffraction. (B) Diffractograms collected at room temperature from samples annealed at 760°C to obtain quartz solid solutions (Qss); (C) similar measurements acquired from samples treated at higher temperatures to crystallize keatite solid solutions (Kss) (labels: q for Qss, k for Kss, s for the weighed-in silicon standard, d for $Li_2Si_2O_5$, m for Li_2SiO_3, c for cristobalite; * marks an artifact stemming from the $L\alpha_1$-line of the tungsten X-ray cathode)

3.3 | Keatite solid solutions

As noted above, a heat treatment at 760°C induced the formation of some Kss in the Li_2O- and Al_2O_3-richer samples, as expected from the thermodynamic stability of this phase and from previous investigations of similar compositions.[8,20,32,35] The lattice parameters obtained at room temperature (the determination was considered reliable only for Kss fractions >25 wt%) agreed closely with the trends known from literature (Figure 3),[10,35] illustrating also in this case how the Al/Si ratio of the base glass directly determined the composition of the obtained crystals.

In addition, we tested the possibility of extending the known solid solution boundaries of Kss, by treating LA10 and LA15 at higher temperature. These samples displayed an evident tendency to form Kss at 760°C, thereby locating substantially beyond the compositional field of previous systematic investigations.[10,35] We therefore tentatively annealed these powders at 1050 and 850°C, increasing their Kss fraction to 44 and 88 wt%, respectively. Due to the expectable partial segregation of SiO_2 in secondary phases such quartz and cristobalite at these higher temperatures,[8] the lattice parameters obtained for Kss in the two samples clearly diverged from the trends reasonably inferable from the extrapolation of literature data in this previously unexplored compositional range.[10,35,36] The values plotted however substantially lower than the references, confirming that a lower degree of Al+Li stuffing was attained. Depending on the assumed adherence to a simple linear trend or to a more complex continuous variation down to the values determined for unstuffed keatite by Shropshire et al., the composition of Kss in the two samples could be estimated as follows: 82.5–83.0 mol% SiO_2 in sample LA15, 84.3–85.4 mol% SiO_2 in sample LA10 (see Figure 3B, i.e. the projected horizontal lines connecting the nominal compositions with the linear and polynomial trends).

3.4 | Thermal expansion behavior

XRD measurements performed in situ at high temperatures (up to 650°C) and under cryogenic conditions (down

inversion temperatures (T_c) in Table 1 agree closely with the values specified in previous works, marked by horizontal broken lines in Figure 4.[20,32,34]

to −165°C) allowed to precisely characterize the thermal expansion of the main crystalline components of the glass-ceramics, namely Qss and Kss. Anisotropic expansion
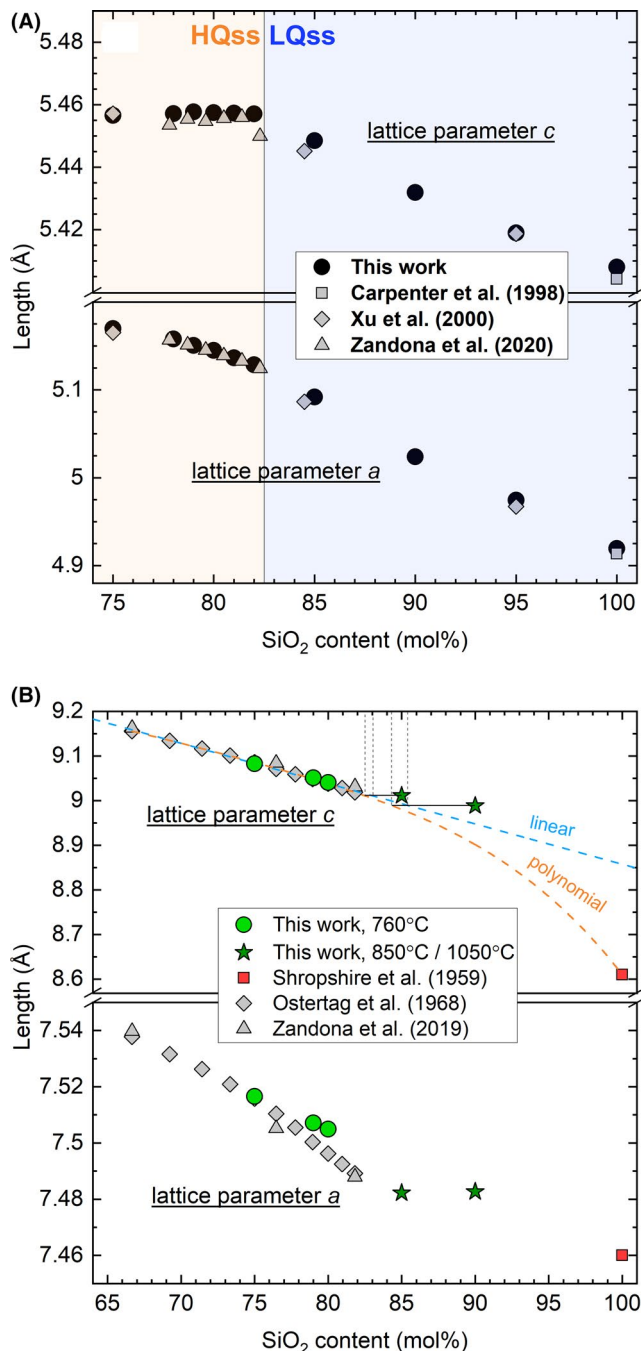

FIGURE 3 Lattice parameters obtained at room temperature for the (A) quartz solid solution and (B) keatite solid solution (Kss) phases crystallized in the samples, plotted as a function of their nominal SiO_2 content. Error bars are smaller than the depicted symbols; values from relevant literature references are provided for comparison.[7,10,32,33,35,36] The extrapolated trends of the *c* lattice parameter (linear: only data from Ostertag et al.; polynomial: data from Ostertag et al. and Shropshire et al.) were used to estimate the actual SiO_2 content of Kss in the samples LA15 and LA10, respectively, treated at 850 and 1050°C

regimes characterized the crystals along *a* and *c*, as known from literature[10,34] and exemplified for Qss in the range −50 to +50°C (Figure 5). Nevertheless, the values of the lattice parameters determined by Rietveld refinement at each temperature (Tables S1 and S2) could be used to calculate an average relative linear expansion of the crystals according to Equation (1). As anticipated, strong positive thermal expansion was invariably observable in the samples containing LQss, gradually increasing its slope until the abrupt transition into HQss, characterized instead by a slight thermal contraction. As the SiO_2 content of the samples reduced, the range of negative/zero thermal expansion enlarged to lower and lower temperature, until full stabilization of HQss in the investigated temperature range was accomplished (samples LA22 and LA25). The closest curve to virtually zero thermal expansion was the one derived in the range 25–650°C for Kss in sample LA15, while the lower Kss content of sample LA10 did not allow a reliable evaluation.

Between −50 and +50°C, the linear CTEs obtainable for Qss phases varied from $+30 \times 10^{-6}$ to $-2.7 \times 10^{-6} \, K^{-1}$, satisfactorily agreeing with the trends extracted from literature.[34] Since all Qss displayed the highest thermal expansion right before the LQss-HQss transition, the CTEs grew as the transformation shifted toward room temperature, from pure SiO_2 to the mentioned threshold of 82.5 mol% SiO_2; at higher levels of Al+Li doping, thermal contraction prevailed. As for Kss in sample LA15, it exhibited a CTE of approximately $-1.0 \times 10^{-6} \, K^{-1}$, again lining up well with the available literature sources.[6,10] (Figure 6).

4 | DISCUSSION

The results of our investigation qualify spray-drying as a very versatile method for the production of glass-ceramic powders in the LAS system. A broad range of compositions, spanning from almost pure silica to less than 75 mol% SiO_2, could be sprayed, calcined, and crystallized without the need of adjusting the experimental procedure in any of its stages. This is particularly impressing if one considers that the obtainment of similar glasses by the melt-quench route involves coping with liquidus temperatures up to 1700°C and very high viscosity, preventing easy pouring and forming.[8,37] On a laboratory scale, the spray-dryer used in this work effectively schematizes the design of large-scale hot-wall reactors already in use for the aerosol production of commercially available ceramic powders,[38] indicating an easy upscalability of this synthesis route. Moreover, our process substantially accelerates the drying and condensation stages as compared to other sol-gel techniques, minimizing the risk of heterogeneities arising in the sol.

The LAS crystals formed in the glass-ceramic powders exhibited CTEs going from slightly negative to strongly positive, allowing free compositional pinpointing of a suitable thermal expansion behavior. We fully demonstrate this tailorability in the case of Qss phases: we were able to produce powders with Qss as the main crystalline phase over the whole studied compositional field, despite the well-known metastability of these phases, obtained by other authors using more complex high-temperature high-pressure synthesis at similar compositions.[39] As for Kss, its formation is rather favored below approximately 80 mol% SiO_2 because of its thermodynamic stability; for this reason, we concentrated our efforts on the metastable enlargement of this compositional range. While sample LA10 yielded a complex crystalline assemblage for locating too deep in the cristobalite+Kss stability field, LA15 could be successfully crystallized prevalently in Kss with a SiO_2 content of 82.5–83.0 mol%. It still remains unclear whether Kss phases could be attainable at even higher SiO_2 contents, given the theoretical complete isostructurality of

β-spodumene and keatite.[36,40] In fact, the clear divergence of the lattice parameters and CTEs from a perfect linear trend down to the pure silica endmember (as shown in Figure 3) suggests a higher complexity of crystallographic relations in this region.

All this considered, the crystallization of spray-dried LAS glasses enabled to easily access an extensive interval of metastable crystalline states (and therefore properties), in addition to the ones favored by thermodynamics. The initial glassy nanobeads were likely to contain some residual water and organics even after a calcination at 500°C, as observed previously in spray-dried SiO_2-TiO_2 glass-ceramics.[30] This volatile content may have effectively lowered glass viscosity, facilitating the initial stages of crystallization and sintering and causing the grain coarsening and agglomeration documented by TEM (Figure 1). Concurrently, we employed an excess of Li_2O to foster the crystallization of the samples into Qss and to suppress the formation of cristobalite, as documented in the past[31]; please note that we demonstrated that Li_2O volatilization
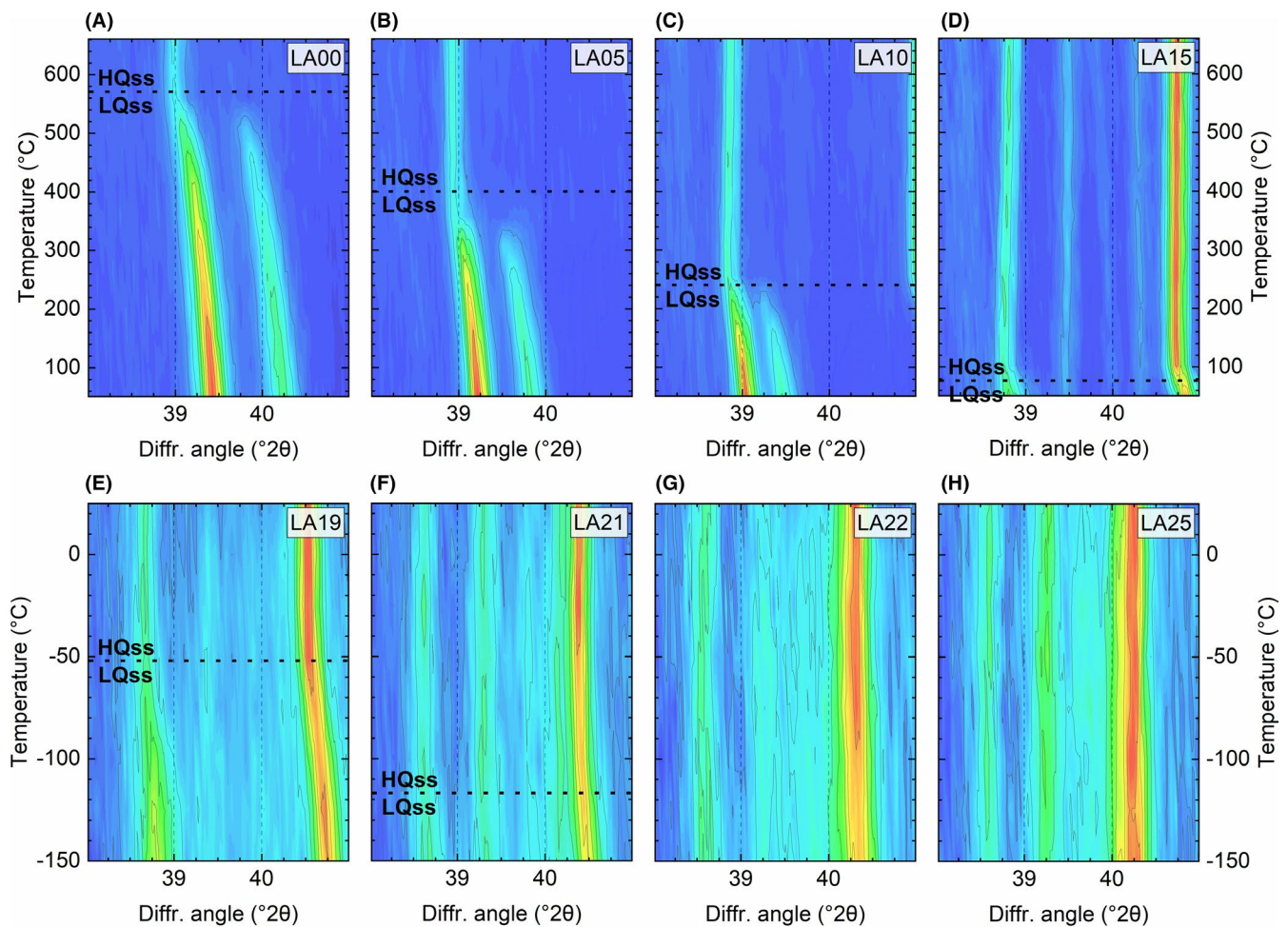

FIGURE 4 Excerpts of the X-ray diffraction measurements performed at high temperature and at cryogenic conditions, manifesting the high-low inversion of quartz solid solution in samples: (A) LA00, (B) LA05, (C) LA10, (D) LA15, (E) LA19, (F) LA21, (G) LA22, (H) LA25. Horizontal lines indicate the expected value of T_c, as from previous studies[20,32,34]
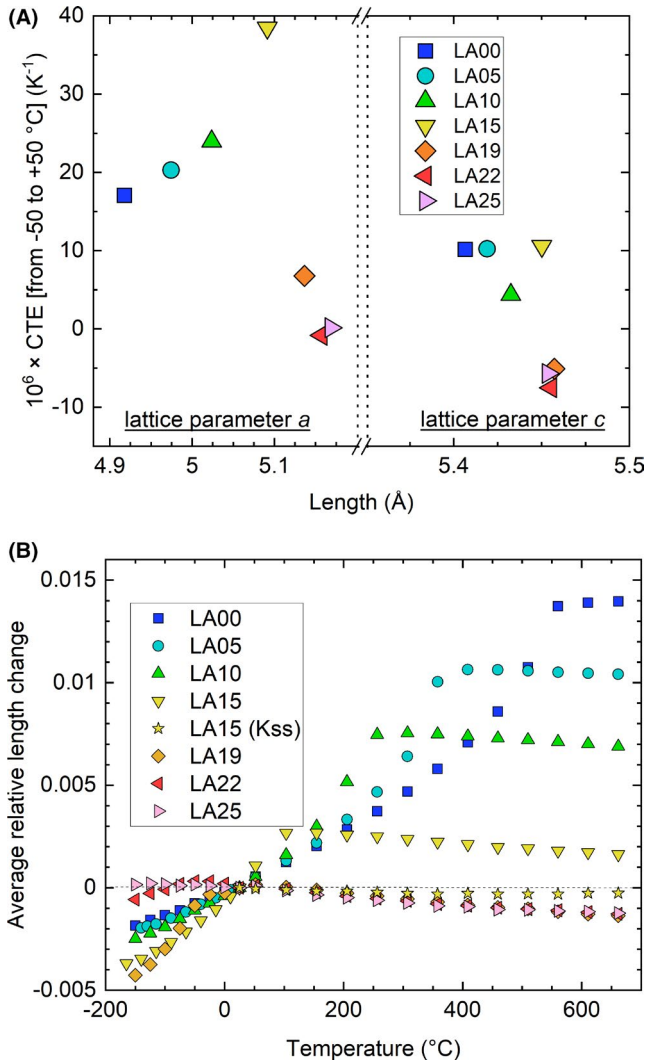
FIGURE 5 (A) Linear coefficient of thermal expansions along the *a* and *c* directions of the quartz solid solution (Qss) crystals (samples LA00, LA05, LA10, LA15, LA19, LA22, LA25 annealed at 760°C), plotted against the respective values of the lattice parameters at room temperature. (B) Relative length change as a function of temperature, averaged over all directions in the unit cell volumes of Qss (see above) and keatite solid solution (sample LA15 annealed at 850°C; the lower amounts contained in the other samples prevented a reliable determination). The length changes were computed by Rietveld refinements of X-ray diffraction measurements acquired between −165 and 650°C. Error bars are smaller than the depicted symbols
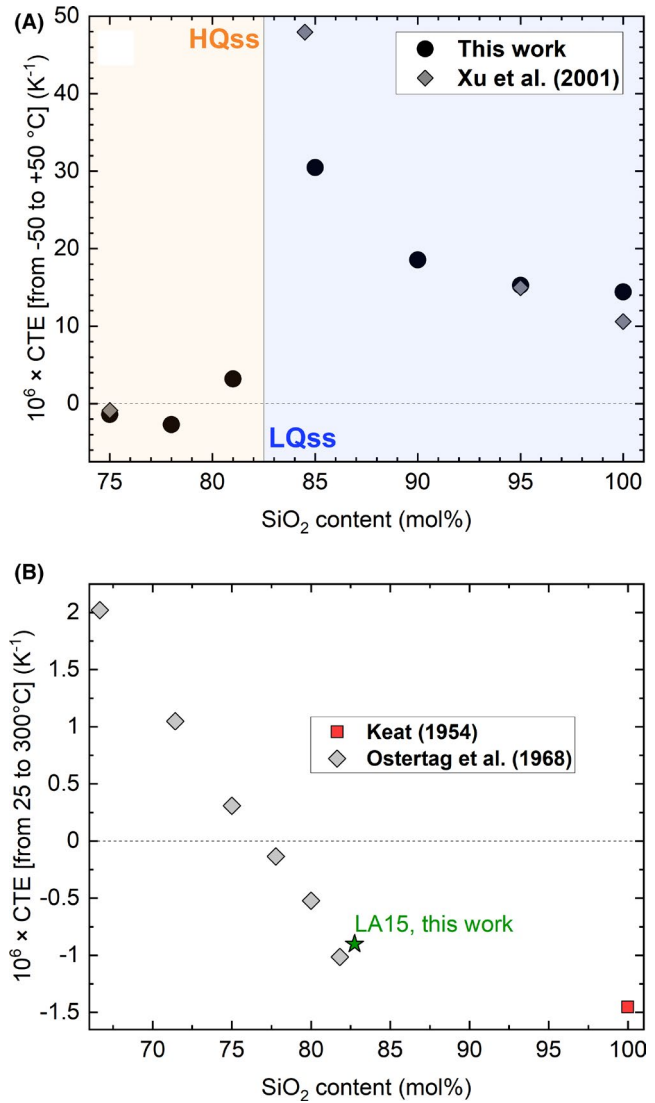
FIGURE 6 Coefficient of thermal expansions computed from the curves shown in Figure 5A for: (A) Quartz solid solution crystals between −50 and +50°C, plotted as a function of their nominal SiO_2 content; (B) keatite solid solution crystals in sample LA15 between 25 and 300°C, plotted as a function of the SiO_2 content inferred from Figure 3. Values obtained from the literature are also reported.[6,10,34] Error bars are smaller than the depicted symbols.

in similar glasses is negligible even for samples melted conventionally at 1650°C.[31,41] The compositional approach used in this work is distinctly different from that of commercial monolithic LAS glass-ceramics, containing a molar excess of Al_2O_3 over the sum ($Li_2O+MgO+ZnO$), a lower amount of SiO_2 and a number of additional components (such TiO_2, ZrO_2 and SnO_2[42,43]) to induce sufficient volume nucleation and control the properties of the residual glassy phase.[12]

In the crystalline state, the Li_2O excess appeared to mostly segregate in the form of Li-metasilicate and Li-disilicate (invariably <5 wt%). Due to these secondary phases, one may hypothesize a slight SiO_2 depletion of the Kss and Qss crystals compared to the target stoichiometry; however, we have estimated the maximum overall expectable deviation as ~0.5 mol% SiO_2, that is, virtually unresolvable by laboratory X-ray diffractometry. In fact, only the Qss forming in LA00 displayed a visible discrepancy in the value of T_c with respect to literature: the inversion temperature of pure quartz is typically located at 573°C, while the sample exhibited zero thermal expansion

starting from the measurement at 550°C. Nevertheless, the inversion temperature of pure quartz is known to be strongly affected by even minor impurity levels[44]; in the other samples, the coupled Al+Li substitution probably prevailed over the possible effect of minor deviations from stoichiometry, yielding a good agreement with the literature references.

5 | CONCLUSION

We demonstrated how "aged" and well-known functional materials, that is, LAS glass ceramics, can acquire an unprecedented compositional versatility if obtained using alternative synthesis methods. Spray-dried glass-ceramic powders enable to access the formation of Qss and Kss crystals with a whole range of compositionally tunable CTEs, from mildly negative to strongly positive.

ORCID
Alessio Zandona https://orcid.org/0000-0003-0091-9546
Joachim Deubener https://orcid.org/0000-0002-3474-7490

REFERENCES
1. Versluis A, Douglas WH, Sakaguchi RL. Thermal expansion coefficient of dental composites measured with strain gauges. Dent Mater. 1996;12(5):290–4.
2. Wong CP, Bollampally RS. Thermal conductivity, elastic modulus, and coefficient of thermal expansion of polymer composites filled with ceramic particles for electronic packaging. J Appl Polym Sci. 1999;74(14):3396–403.
3. Chu CN, Saka N, Suh NP. Negative thermal expansion ceramics: a review. Mater Sci Eng. 1987;1(95):303–8.
4. Miller W, Smith CW, Mackenzie DS, Evans KE. Negative thermal expansion: a review. J Mater Sci. 2009;44(20):5441–51.
5. Hummel FA. Thermal expansion properties of some synthetic lithia minerals. J Am Ceram Soc. 1951;34(8):235–9.
6. Keat PP. A new crystalline silica. Science. 1954;120(3113):328–30.
7. Carpenter MA, Salje EKH, Graeme-Barber A, Wruck B, Dove MT, Knight KS. Calibration of excess thermodynamic properties and elastic constant variations associated with the alpha ↔ beta phase transition in quartz. Am Miner. 1998;83(1–2):2–22.
8. Roy R, Roy DM, Osborn EF. Compositional and stability relationships among the lithium aluminosilicates: eucryptite, spodumene, and petalite. J Am Ceram Soc. 1950;33(5):152–9.
9. Li C-T. The role of lithium in stabilizing some high-temperature silica phases. Z Kristallogr Cryst Mater. 1973;138(1–6):216–36.
10. Ostertag W, Fischer GR, Williams JP. Thermal expansion of synthetic β-Spodumene and β-Spodumene—silica solid solutions. J Am Ceram Soc. 1968;51(11):651–4.
11. Petzoldt J. Metastabile Mischkristalle mit Quarzstruktur mit Oxidsystem Li₂O-MgO-ZnO-Al₂O₃-SiO₂. Glastechn Ber. 1967;40(10):385–95.
12. Krause D, Bach H, editors. Low thermal expansion glass ceramics. Berlin Heidelberg: Springer; 2005. (Schott Series on Glass and Glass Ceramics).
13. Hochella MF Jr, Brown GE Jr. Structural mechanisms of anomalous thermal expansion of cordierite-beryl and other framework silicates. J Am Ceram Soc. 1986;69(1):13–8.
14. Zandona A, Rüdinger B, Deubener J. Mg-bearing quartz solid solutions as structural intermediates between low and high quartz. J Am Ceram Soc. 2021;104(2):1146–55.
15. Bruneton E, Bigarre J, Michel D, Colomban P. Heterogeneity, nucleation, shrinkage and bloating in sol–gel glass ceramics (the case of lithium aluminosilicate compositions). J Mater Sci. 1997;32(13):3541–8.
16. Jang HM, Kim KS, Jung CJ. Chemical processing and densification characteristics of lithium aluminosilicate (LAS) gels. J Mater Res. 1992;7(8):2273–80.
17. Xia L, Wen GW, Qin CL, Wang XY, Song L. Mechanical and thermal expansion properties of β-eucryptite prepared by sol–gel methods and hot pressing. Mater Des. 2011;32(5):2526–31.
18. Lee GS, Messing GL, Delaat FGA. Crystallization of sol-gel-derived lithium aluminosilicate (LAS) glass ceramic powders. J Non-Cryst Solids. 1990;116(2):125–32.
19. Anderson P, Klein LC. Shrinkage of lithium aluminosilicate gels during drying. J Non-Cryst Solids. 1987;93(2):415–22.
20. Helsch G, Deubener J, Rampf M, Dittmer M, Ritzberger C. Crystallization and quartz inversion temperature of sol-gel derived LAS solid solutions. J Non-Cryst Solids. 2018;15(492):130–9.
21. Arpagaus C, Collenberg A, Rütti D, Assadpour E, Jafari SM. Nano spray drying for encapsulation of pharmaceuticals. Int J Pharm. 2018;546(1):194–214.
22. Martínez Arias A, Weber AP. Aerosol synthesis of porous SiO₂-cobalt-catalyst with tailored pores and tunable metal particle size for Fischer-Tropsch synthesis (FTS). J Aerosol Sci. 2019;1(131):1–12.
23. Belbekhouche S, Poostforooshan J, Shaban M, Ferrara B, Alphonse V, Cascone I, et al. Fabrication of large pore mesoporous silica microspheres by salt-assisted spray-drying method for enhanced antibacterial activity and pancreatic cancer treatment. Int J Pharm. 2020;590:119930.
24. Gharsallaoui A, Roudaut G, Chambin O, Voilley A, Saurel R. Applications of spray-drying in microencapsulation of food ingredients: an overview. Food Res Int. 2007;40(9):1107–21.
25. Saadaldin SA, Rizkalla AS. Synthesis and characterization of wollastonite glass–ceramics for dental implant applications. Dent Mater. 2014;30(3):364–71.
26. Molino G, Bari A, Baino F, Fiorilli S, Vitale-Brovarone C. Electrophoretic deposition of spray-dried Sr-containing mesoporous bioactive glass spheres on glass–ceramic scaffolds for bone tissue regeneration. J Mater Sci. 2017;52(15):9103–14.
27. Kortesuo P, Ahola M, Kangas M, Kangasniemi I, Yli-Urpo A, Kiesvaara J. In vitro evaluation of sol–gel processed spray dried silica gel microspheres as carrier in controlled drug delivery. Int J Pharm. 2000;200(2):223–9.

28. Douy A, Canale P, Coutures J. Spray-dried homogeneous cordierite and MLAS glass-ceramic powders. J Eur Ceram Soc. 1992;9(5):373–80.

29. Jaymes I, Douy A. Homogeneous mullite-forming powders from spray-drying aqueous solutions. J Am Ceram Soc. 1992;75(11):3154–6.

30. Zandona A, Martínez Arias A, Gutbrod M, Helsch G, Weber AP, Deubener J. Spray-dried TiO_2(B)-containing photocatalytic glass-ceramic nanobeads. Adv Funct Mater. 2020;20:2007760.

31. Zandona A, Helsch G, Al-Mukadam R, Deubener J. The effects of a Li_2O excess on the crystallization sequence of lithium aluminosilicate glass powders. J Non-Cryst Solids. 2021;561:120748.

32. Zandona A, Helsch G, Deubener J. Inversion of quartz solid solutions at cryogenic temperatures. J Am Ceram Soc. 2020;103(11):6630–8.

33. Xu H, Heaney PJ, Beall GH. Phase transitions induced by solid solution in stuffed derivatives of quartz: a powder synchrotron XRD study of the $LiAlSiO_4$-SiO_2 join. Am Miner. 2000;85(7):971–9.

34. Xu H, Heaney PJ, Navrotsky A. Thermal expansion and structural transformations of stuffed derivatives of quartz along the $LiAlSiO_4$–SiO_2 join: a variable-temperature powder synchrotron XRD study. Phys Chem Miner. 2001;28(5):302–12.

35. Zandona A, Rüdinger B, Hochrein O, Deubener J. Crystallization sequence within the keatite solid solution – cordierite mixed compositional triangle with TiO_2 as nucleating agent. J Non-Cryst Solids. 2019;1(505):320–32.

36. Shropshire J, Keat PP, Vaughan PA. The crystal structure of keatite, a new form of silica. Z Kristallogr Cryst Mater. 1959;112:409–13.

37. Rustum R, Osborn EF. The system lithium metasilicate–spodumene–silica. J Am Chem Soc. 1949;71(6):2086–95.

38. Buesser B, Pratsinis SE. Design of nanomaterial synthesis by aerosol processes. Annu Rev Chem Biomol Eng. 2012;3:103–27.

39. Xu H, Heaney PJ, Navrotsky A, Topor L, Liu J. Thermochemistry of stuffed quartz-derivative phases along the join $LiAlSiO_4$-SiO_2. Am Miner. 1999;84(9):1360–9.

40. Li C-T, Peacor DR. The crystal structure of $LiAlSi_2O_6$-II ("β spodumene"). Z Kristallogr Cryst Mater. 1968;126(1–3):46–65.

41. Zandona A, Patzig C, Rüdinger B, Hochrein O, Deubener J. TiO_2(B) nanocrystals in Ti-doped lithium aluminosilicate glasses. J Non-Cryst Solids X. 2019;1(2):100025.

42. Dressler M, Rüdinger B, Deubener J. An in situ high-temperature X-ray diffraction study of early-stage crystallization in lithium alumosilicate glass-ceramics. J Am Ceram Soc. 2011;94(5):1421–6.

43. Dressler M, Rüdinger B, Deubener J. Crystallization kinetics in a lithium alumosilicate glass using SnO_2 and ZrO_2 additives. J Non-Cryst Solids. 2014;1(389):60–5.

44. Keith ML, Tuttle OF. Significance of variation in the high-low inversion of quartz. Am J Sci. 1952;Bowen:203–80.

SUPPORTING INFORMATION

Additional supporting information may be found online in the Supporting Information section.